Supporting Information

Unidirectional/bidirectional Electron Transfer at the Au/TiO_2 Interface Operando Tracked by SERS Spectra from Au and TiO_2

*Xinlu Zheng, Xuefeng Yan, Jiayu Ma, Xinyun Yao, Jinlong Zhang, and Lingzhi Wang**

Key Laboratory for Advanced Materials and Feringa Nobel Prize Scientist Joint Research Center, Institute of Fine Chemicals, School of Chemistry and Molecular Engineering, East China University of Science & Technology, 130 Meilong Road, Shanghai, 200237, China

Corresponding Author
*wlz@ecust.edu.cn

Outlines

Part I: Experimental Section

Chemicals

Acetylacetone, Tetraethyl orthosilicate (TEOS) and HCl were purchased from Shanghai Lingfeng Chemical Reagent Co. Ltd without further purification. Ethanol was purchased from Shanghai Chemical Reagent. Titanium isopropoxide (TTIP) and 4-nitrothiophenol (PNTP) were purchased from Aladdin. Ultrapure water (=18.0 MΩ) purified using the Milipore Milli-Q gradient system.

Characterizations: X-ray powder diffraction (XRD) is analyzed on Rigaku D/max 2250 VB/PC apparatus. Scanning electron microscopy (SEM) images are obtained on TESCAN nova 3. Transmission electron microscopy (TEM) images are recorded on JEOL JEM-2100. UV-Vis spectra are measured on UV-Vis spectrophotometer (Shimadzu UV-2450).

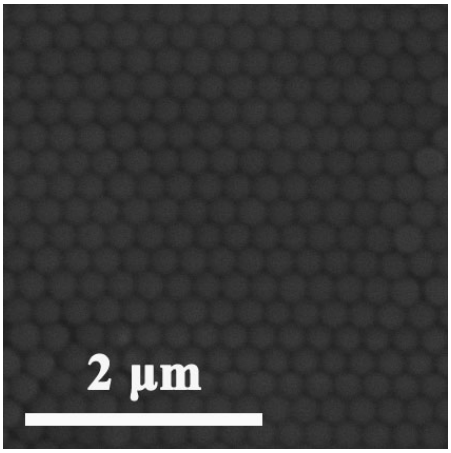

Figure S1. SEM of polystyrene (PS) microarray.

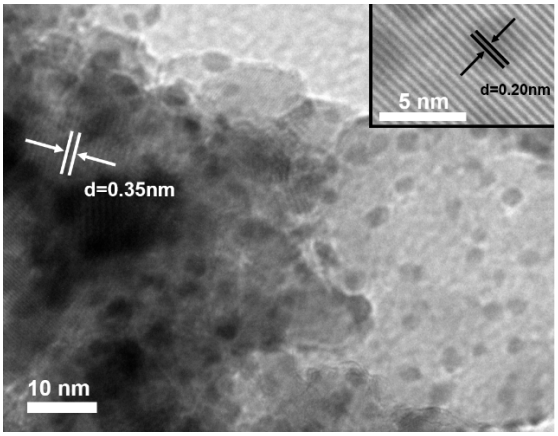

Figure S2. HRTEM of Au-2/TiO_2 composite.

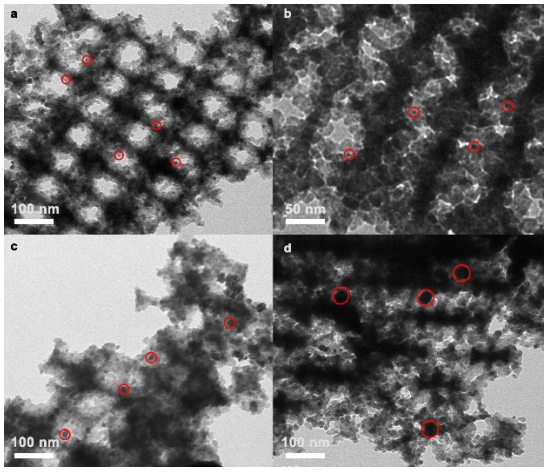

Figure S3. TEM of (a) Au-2/TiO_2, (b) Au-7/TiO_2, (c) Au-15/TiO_2 and (d) Au-23/TiO_2.

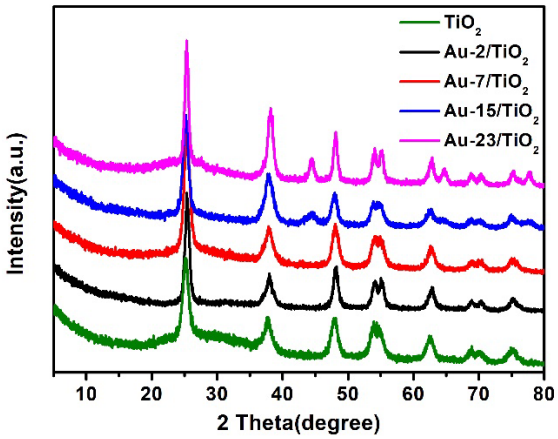

Figure S4. XRD patterns of TiO_2 and different Au/TiO_2 composites.

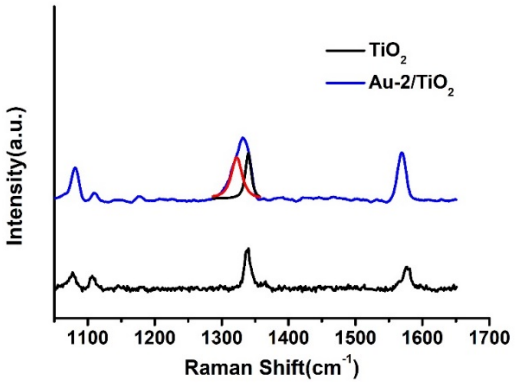

Figure S5. SERS spectra of PNTP obtained from IO TiO_2 and Au-2/TiO_2.

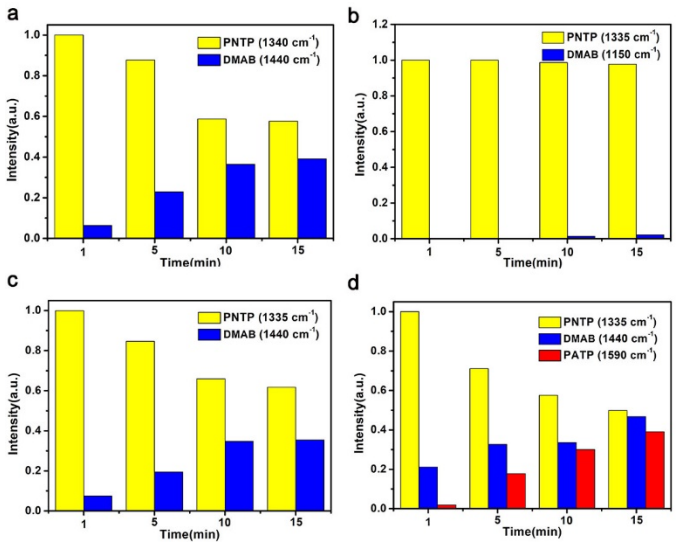

Figure S6. The relationship of the Raman intensity versus irradiation time on (a) Au-2/TiO_2 (b) Au-7/TiO_2 (c) Au-15/TiO_2 and (d) Au-23/TiO_2. (The peaks at 1150 cm^{-1} and 1440 cm^{-1} are attributed to the β(C-H) and the azo group of DMAB, respectively.)

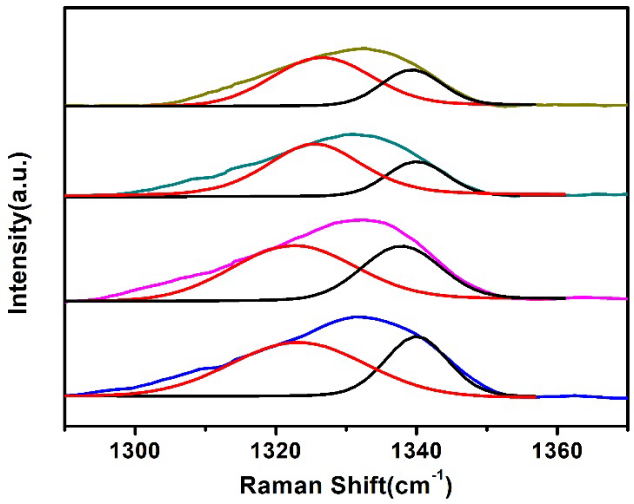

Figure S7. Magnified SERS spectra of PNTP adsorbed on Au-2/TiO_2 between 1290 and 1370 cm^{-1} (red and black curves are peak fitting results using Gauss-Lorentzian peak shapes). During the process of peak-fitting, the position and the full width at half maximum (FWHM) belonging to the molecules adsorbed on TiO_2 should be kept

relatively fixed. And under this premise, the other peak attributed to the stretching vibration mode of -NO_2 on Au surface environment is naturally set.

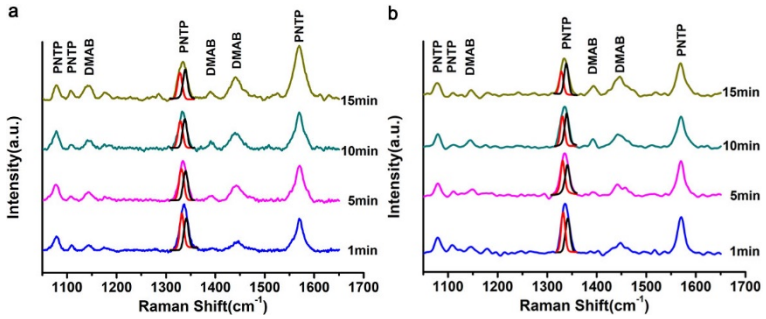

Figure S8. SERS spectra of PNTP on (a) Au-15/SiO_2 and (b)Au-23/SiO_2 under continous irradiation of 532 nm laser.

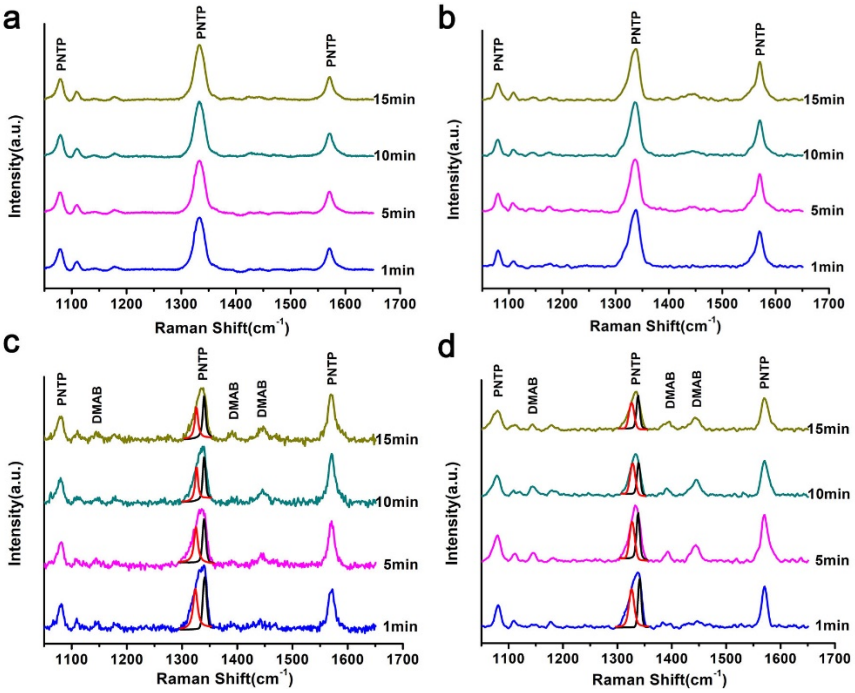

Figure S9. *In situ* SERS spectra of PNTP on (a) Au-2/TiO_2, (b) Au-7/TiO_2, (c) Au-15/TiO_2 and (d) Au-23/TiO_2 under irradiation of 633 nm laser.

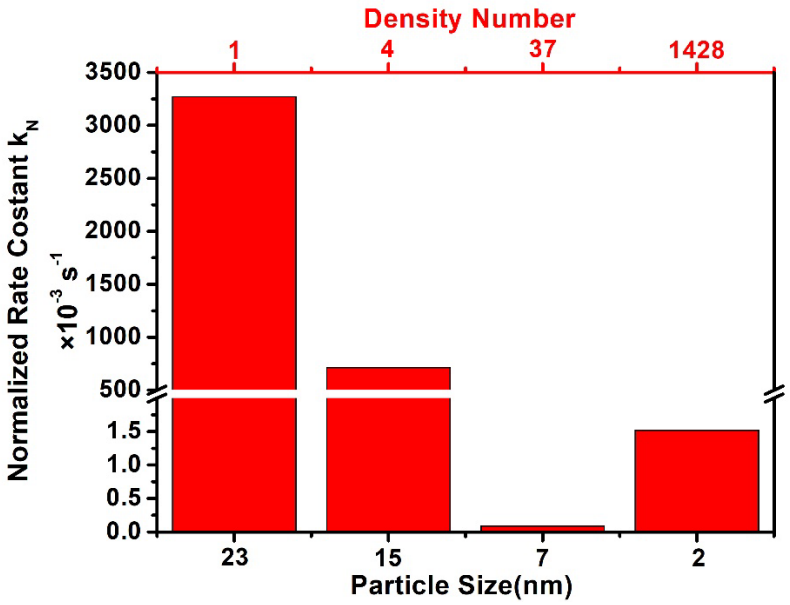

Figure S10. Rate constant normalized to the density number of Au nanoparticles.

The rate constants of all Au/TiO_2 composites are normalized taking the density number of Au-2/TiO_2 composite as a reference. Since the total mass of Au is same, as the particle size is increased, the density number of Au particles will decrease greatly. In this case, the normalized rate constant of larger size Au presents much bigger than the smaller one.

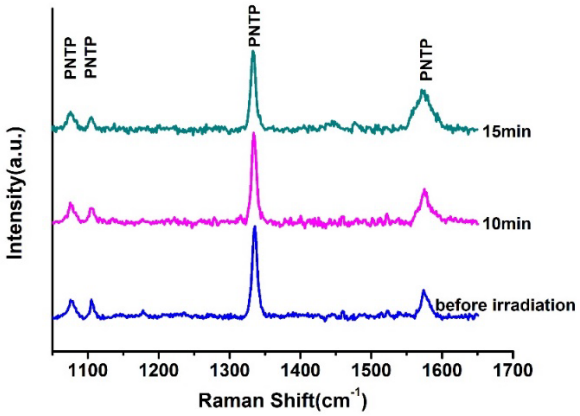

Figure S11. SERS spectra of PNTP on pure TiO_2 under UV irradiation.

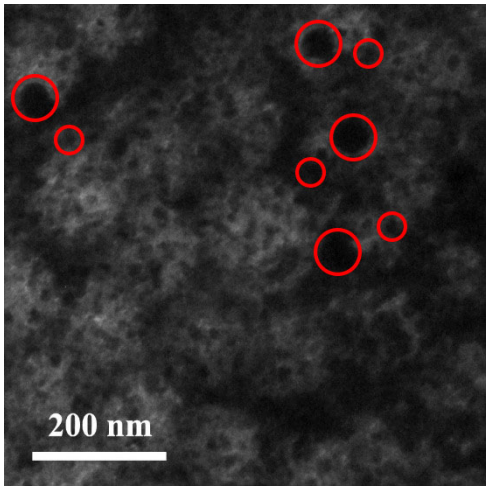

Figure S12. TEM of dual-sized Au-23-7/TiO_2.

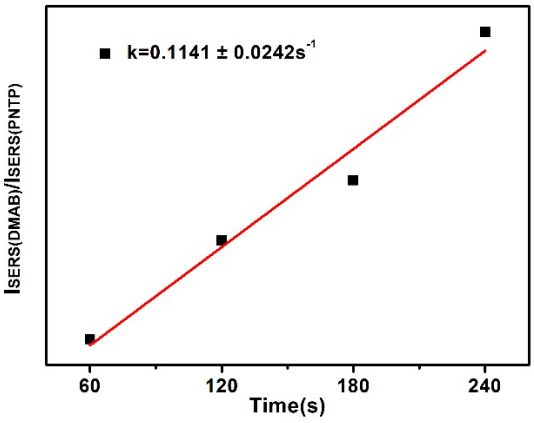

Figure S13. The dynamic analysis of dual-sized Au-23-7/TiO_2 composite.

Part II: The relation between atom number and contact area

The total atom numbers of each Au particle was calculated using truncated octahedron as the model. For example, the Au NPs with the sizes of 2 and 7 nm have atom numbers of ca. 286 and 11018. Using the half truncated octahedron Au NP as the adsorption model, the interfacial atom numbers are almost 70% reduced due to the increasing particle size.

Table S1 Formulas for calculations of Au size, particle numbers, the atom numbers in each Au particle and the contact area at the Au/TiO_2 interface

Total atom number of each particle (N_T)	$16m^3-33m^2+24m-6$
Number of Au particles (N_P)	$N_{Au} \bullet N_A/N_T$
Size of Au NPs (d)	$1.105 * N_T^{1/3} * d_{Au\ atom}$
Interfacial atom numbers for each half truncated octahedron Au paticles (N_I)	$5m^2-6m+2$

Here, the m in the formula is the number of atoms lying on an equivalent edge (corner atoms included), N_A is the Avogadro constant and the diameter of Au atom ($d_{Au\ atom}$) is 0.292 nm.[1] The total interfacial atom numbers are calculated by multiplying N_P and N_I.

Part III: The width of space charge layer (w)

The space charge layer (SCL) or the depletion layer width (w) can be determined as equation (1), which is proportional to the built-in potential or the barrier height and will be widened when a negative bias pointed from TiO_2 to Au is applied. The UV irradiation before 532 nm laser is similar to apply a negative bias at the interface, which can widen the SCL and is detrimental to the subsequent LSPR-induced electron transfer before a new equilibrium is reached. Moreover, since Au-2 capped with -SH group has a lower

barrier height,[2] the barrier width is also narrower than the other composites. The improved contact area with the decreasing particle size further helps the electron transfer from Au-2 to TiO_2. In contrast, the wider SCL in other composites with larger Au will consume more hot electrons initially transferred from Au to TiO_2, preventing the reduction of PNTP to DMAB.

$$w = \left\{-\frac{2\varepsilon[V_{bi}+V]}{qN_D}\right\}^{1/2} \quad \text{.....(1)}$$

Here, ε is the permittivity, q is the elementary charge, N_D is the doping density, V and V_{bi} are the applied bias voltage and the built-in potential.

On one hand, according to the reference,[3] the effective density of states in the conduction band of titanium (N_c) equals:

$$N_c = 2\left(\frac{2\pi m_k^* kT}{h^2}\right)^{3/2} \quad \text{.....(2)}$$

Where m_k^* is effective mass of electron, k is the Boltzmann constant, T represents room temperature, and h is Planck constant, substituting these values into equation (2), we obtained:

$$N_c = 2\times\left(\frac{2\pi\times 9\times 10^{-31}\times 1.38\times 10^{-23}\times 300}{(6.626\times 10^{-34})^2}\right)^{3/2}$$

$$= 1.55\times 10^{30}$$

The Mott-Schottky barrier height equals:

$\Phi B = \Phi M - \chi$

Where ΦM is the work fuction of the metal and χ is the electron affinity. Based on the data (The work function of Au is 5.1 eV and electron affinity of TiO_2 is 4.2 eV.[4]), the barrier height is obtained according to the following calculation:

$\Phi B = \Phi M - \chi = 5.1 - 4.2 = 0.9$ eV

The free electron concentration (N_d) was calculated from the equation:[5]

$$N_d = \frac{2C^2}{e\xi_0\xi_r A^2} \quad \text{.....(3)}$$

where C is the interfacial capacitance between the semiconductor and the electrolyte, A is the interfacial area (1 cm^2), e is the electron charge, ε_0 is the vacuum permittivity, ε_r is the relative permittivity of anatase TiO_2 at 1 kHz frequency.[6] The slope of the

straight line of $1/C^2$ is ca. 6.87×10^9 cm^4/F^2 (Figure S12). According to the equation (3), N_d of TiO_2 is calculated to be ca. 7.38×10^{20} The built-in potential equals:

$$\Phi 1=\Phi B\text{-}Vt\ \ln\frac{Nc}{Nd}=0.9\text{-}0.0259\ln\frac{1.55\times10^{30}}{7.38\times10^{20}}=0.35\ eV$$

The total potential difference across the semiconductor equals the built-in potential, in thermal equilibrium and is further reduced/increased by the applied voltage (V_a) when a positive/negative voltage is applied to the metal. This boundary condition provides the following relation between the semiconductor potential at the surface, the applied voltage and the depletion layer width:

$$\Phi 1\text{-}Va=-\Phi(x=0)=\frac{qN_dx_d^2}{2\xi_r}$$

So, the depletion layer width, x_d, yields:

$$x_d=\sqrt{\frac{2\xi_r(\Phi1-Va)}{qN_d}} \quad \text{.....(4)}$$

where ε_r is the relative permittivity of anatase TiO_2 at 1 kHz frequency, q is the quantity of electron charge, substituting these values into equation (4), we obtained:

$$x_d=\sqrt{\frac{2\xi_r\times0.35}{1.602\times10^{-19}\times7.38\times10^{20}}}=0.4\ nm$$

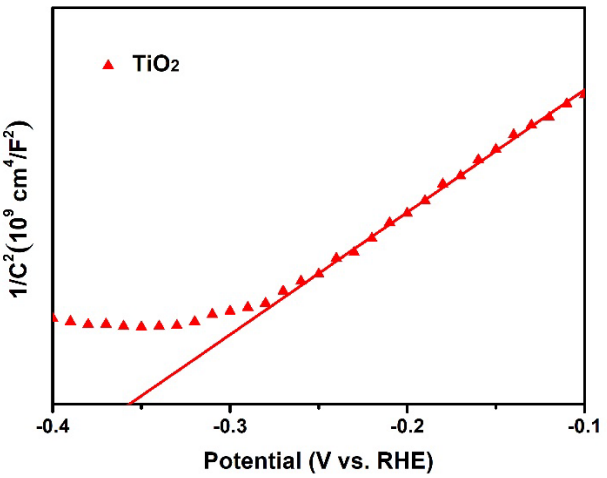

Figure S14. Mott-Schottky plot of TiO_2 measured under visible light irradiation.

Moreover, when Au NPs are loaded on IO TiO_2, the amount of oxygen vacancies (V_O) will be increased, which is confirmed by the XPS result. As shown in Figure S13a, the bingding energies of the typical peak of Ti $2p_{3/2}$ for pure TiO_2 and Au-23/TiO_2 appeared at 458.60 and 458.30 eV, respectively, suggesting that the oxidation state of Ti decreased after the loading of Au. Such behavior probably comes from the patial

reduction of Ti^{4+} by localized electrons at V_O sites.[5] Figure S13b,c shows that the O 1s spectra of pure TiO_2 and Au-23/TiO_2 contained three peaks at 530.1, 531.5 and 532.6 eV that were attributed to O atoms associated with lattice oxygen of TiO_2, neighboring V_O and surface Ti-OH species, respectively.[7] It is worth noting that the peak intensity at 531.5 eV increases after the Au NPs are loaded on TiO_2, suggesting the amount of V_O is increased greatly. Under this circustmance, the electronic structure of TiO_2 can be changed and the energy levels of the introduced localized oxygen vacancy ststes are ca. 0.75 to 1.18 eV below the conduction band edge of TiO_2.[8] As a result, the height of the Mott-Schttky junction will decrease in a degree due to the existence of V_O. When the LSPR-induced electrons are attracted to TiO_2 side by the internal electric field formed at the M-S junction, those that cannot freely and immediately diffuse away from the interface may temporarily accumulate in the positive SCL zone. The situation is similar to applying a positive bias pointing from Au to TiO_2, leading to the reduced height and thickness of the M-S barrier. Based on the above discussion, the theoretical calculation of the depletion layer width under the static mode is ca. 0.4 nm, and when the irradiation is conducted on the system, the height of the M-S junction will be smaller due to the existence of the oxygen vacancy and the irradiation, which stays dynamically changing all the time. In addition, the wall of IO TiO_2 observed from field emission electron scanning microscope (FESEM) has a thickness of approximately 20 nm, which is much larger than that of the width of SCL (Figure S14). Based on the above discussion, it is believed that SCL plays a decisive role in the reaction system, and the built-in electric field promote the charge transfer efficiency at Au/TiO_2 interface.

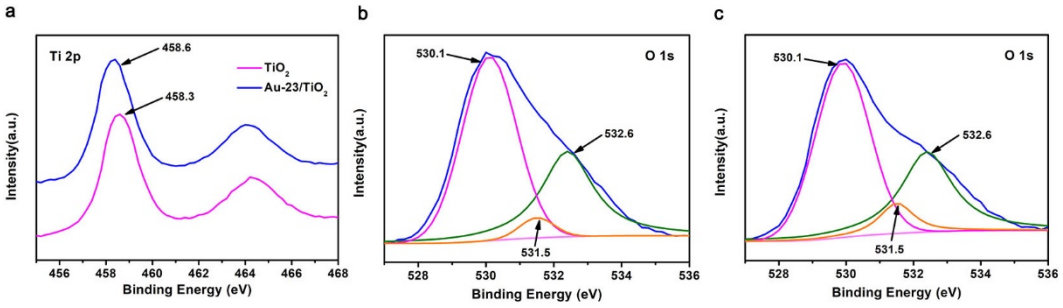

Figure S15. (a) XPS spectra of Ti 2p (TiO_2 and Au-23/TiO_2 composites). XPS spectra of O 1s for (b) IO TiO_2 and (c) Au-23/TiO_2 composite.

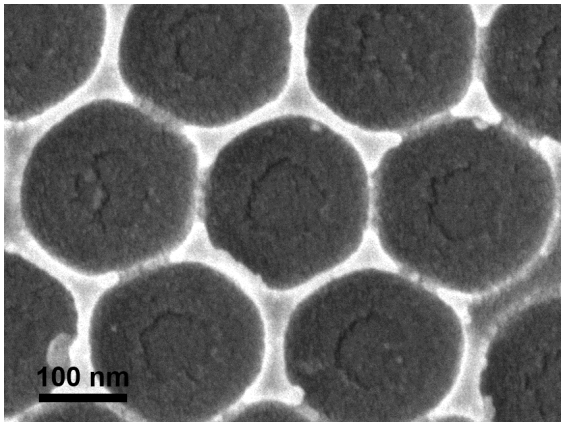

Figure S16. FESEM of IO TiO_2.

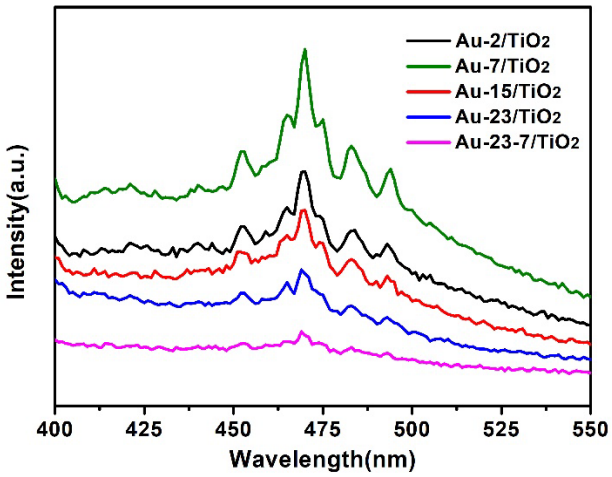

Figure S17. Photoluminescence (PL) spectra of different Au/TiO_2 composites.

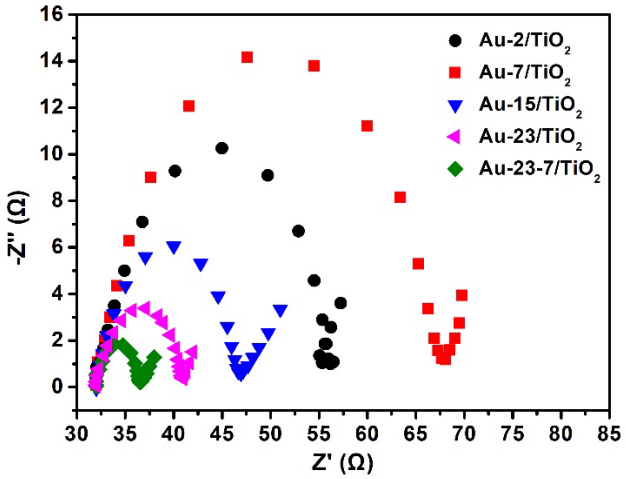

Figure S18. Nyquist diagrams of different Au/TiO_2 composites.

Reference

(1) Zhang, H.; Watanabe, T.; Okumura, M.; Haruta, M.; Toshima, N. Catalytically highly active top gold atom on palladium nanocluster. *Nat. mater.* **2012**, *11*, 49-52.

(2) Mubeen, S.; Zhang, T.; Chartuprayoon, N.; Rheem, Y.; Mulchandani, A.; Myung, N. V.; Deshusses, M. A. Sensitive Detection of H_2S Using Gold Nanoparticle Decorated Single-Walled Carbon Nanotubes. *Anal. Chem.* **2010**, *82*, 250-257.

(3) Lauer, R. B. Electron effective mass and conduction-band effective density of states in $Bi_{12}SiO_{20}$. *J. Appl. Phys.* **1974**, *45*, 1794-1797.

(4) Park, J. Y.; Lee, H.; Renzas, J. R.; Zhang, Y.; Somorjai, G. A. Probing hot electron flow generated on Pt nanoparticles with Au/TiO_2 Schottky diodes during catalytic CO oxidation. *Nano Lett.* **2008**, *8*, 2388-2392.

(5) Yang, J.; Guo, Y.; Jiang, R.; Qin, F.; Zhang, H.; Lu, W.; Wang, J.; Yu, J. C. High-efficiency "working-in-tandem" nitrogen photofixation achieved by assembling plasmonic gold nanocrystals on ultrathin titania nanosheets. *J. Am. Chem. Soc.* **2018**, *140*, 8497-8508.

(6) Kalaiarasi, S.; Jose. M. Dielectric functionalities of anatase phase titanium dioxide nanocrystals synthesized using water-soluble complexes. *Appl. Phys. A* **2017**, *123*, 512-521.

(7) Kruse, N.; Chenakin, S. XPS characterization of Au/TiO_2 catalysts: binding energy assessment and irradiation effects. *Appl. Catal. A: Ge*n. **2011**, *391*, 367-376.

(8) Nakamura, I,; N.; Shuzo, K.; Tatsuhiko, I.; Shinichi, S.; Koji, T. Role of oxygen vacancy in the plasma-treated TiO_2 photocatalyst with visible light activity for NO removal. *J. Mol. Catal. A-Ch*em. **2000**, *161*, 205-212.